Inorganic Chemistry

Article

pubs.acs.org/IC

Two Types of Heterometallic One-Dimensional Alignment Composed of Acetamidate-Bridged Dirhodium and Pivalamidate-Bridged Diplatinum Complexes

Kazuhiro Uemura,* Toru Kanbara, and Masahiro Ebihara

Department of Chemistry and Biomolecular Science, Faculty of Engineering, Gifu University, Yanagido 1-1, Gifu 501-1193, Japan

Supporting Information

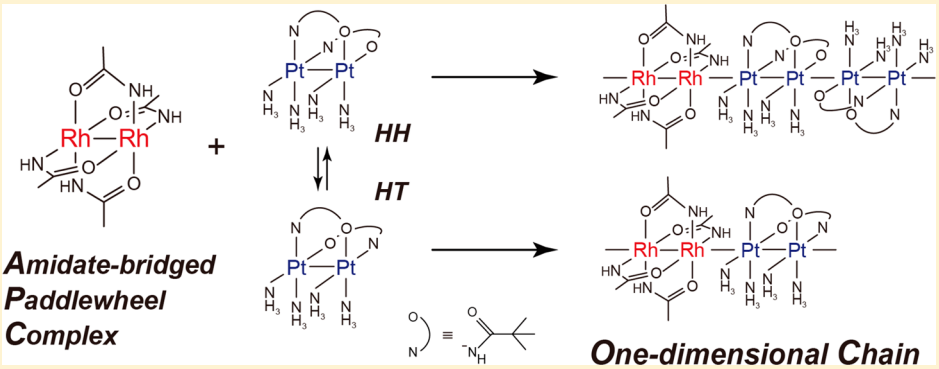

ABSTRACT: Two types of heterometallic one-dimensional chains, $[\{Rh_2(acam)_4\}\{Pt_2(piam)_2(NH_3)_4\}_2]_n(CF_3SO_3)_{4n}\cdot 2n$MeOH (**2**, where acam = acetamidate, piam = pivalamidate) and $[\{Rh_2(acam)_4\}\{Pt_2(piam)_2(NH_3)_4\}]_n(CF_3CO_2)_{2n}\cdot 2n$EtOH (**3**), have been synthesized and characterized by single-crystal X-ray analyses. The chain structures in **2** and **3** are composed of two kinds of dinuclear complexes, $[Rh_2(acam)_4]$ (i.e., $[Rh_2]$) and $[Pt_2(piam)_2(NH_3)_4]$ (i.e., $[Pt_2]$), where Rh and Pt atoms are axially linked by metal−metal bonds. In **2** and **3**, each complex is one-dimensionally aligned as $-\{[Rh_2]-[Pt_2]-[Pt_2]\}_n-$ or $-\{[Rh_2]-[Pt_2]\}_n-$, respectively, in which different alignments are caused by different isomers of $[Pt_2]$ that are HH (head−head) and HT (head−tail) orientation of piam ligands and their hydrogen bonding modes. Considering the crystal structures and X-ray photoelectron spectra (XPS) measurements in **2** and **3**, the oxidation states of the metal atoms are $-\{[Rh_2^{II,II}]-[Pt_2^{II,II}]-[Pt_2^{II,II}]\}_n-$ and $-\{[Rh_2^{II,II}]-[Pt_2^{II,II}]\}_n-$, which are unchanged from those in the starting compounds. The diffuse reflectance spectra show that LUMOs are M−M σ-type orbitals. The gap between filled and vacant σ-type orbitals in **3** is narrower than that in **2**, and is attributed to the relative higher destabilized filled σ-type orbitals caused by lower numbers of linking platinum atoms.

INTRODUCTION

One-dimensional (1D) metal complexes have attracted the attention of researchers for several decades because of their unusual electrical and physical properties,[1−6] including progressive resonance Raman spectra and large third-order nonlinear optical properties.[4] Several compounds consisting of −M−M− bonds[7−16] and a large number of halogen-bridged −M−X− or −M−M−X− chains[17−22] have been synthesized and investigated. The synthetic approach for infinite chains depends on the metal oxidation states; half-filled (d^7) and filled (d^8) d_{z^2} orbitals on the metal atoms are superimposed to form σ-type orbitals, and those are infinitely crystallized. Therefore, syntheses for most infinite 1D metal complexes have made use of $Rh^{+/2+}$,[7−11] $Pd^{2+/3+}$,[12,13] and/or $Pt^{2+/3+}$,[14−16] where partial occupation of the d_{z^2} orbitals by oxidation or reduction is utilized, indicating that the highest occupied molecular orbital (HOMO) in ordinary chains is σ-type orbitals. By contrast, in recently reported heterometallic chains,[23,24] which are aligned as −[Pt−Rh]−[Pt−Pt]−[Pt−Pt]−[Rh−Pt]−Cl−, HOMO is δ^* in the [Pt−Rh] moieties, where one unpaired spin hops from one δ^* to the other in the octametallic unit. This was the first example for directly metal−metal bonded 1D chains possessing a non-σ-type orbital as HOMO, anticipating further electronic modulation based on heterometallic −M−M′− bonds.[25−31]

Previously, we have succeeded in obtaining $[\{Rh_2(O_2CCH_3)_4\}\{Pt_2(piam)_2(NH_3)_4\}_2]_n(PF_6)_{4n}\cdot 6nH_2O$ (**1**, where piam = pivalamidate) and analogues consisting of $[Rh_2(O_2CCH_3)_4]$ and various modified platinum complexes.[32−34] In those compounds, vacant σ^* in $[Rh_2(O_2CCH_3)_4]$ and filled σ^* in platinum complexes are effectively overlapped to form unbridged Rh−Pt bonds, resulting in extended heterometallic 1D chains. Interestingly, it is possible to modify ligands not only in platinum parts, but also in rhodium parts, where the (2,2)-*cis*-$[Rh_2(acam)_4]$ (i.e.,

Received: February 6, 2014
Published: April 24, 2014

   dx.doi.org/10.1021/ic500305n | *Inorg. Chem.* 2014, 53, 4621−4628

$[Rh_2]$, where acam = acetamidate)[35] is also bridged by $[Pt_2(piam)_2(NH_3)_4]$ (i.e., $[Pt_2]$) to afford heterometallic 1D chains with similar $-\{[Pt_2]-[Rh_2]-[Pt_2]\}_n-$ repetition.[32] Because the π^* HOMO in $[Rh_2(O_2CCH_3)_4]$ is distinct from that in $[Rh_2(acam)_4]$ where the δ^* orbital results from destabilization by the π interaction with the amidate ligands (Scheme 1),[36] distinct electronic structures are expected in heterometallic 1D chains of $-\{[Pt_2]-[Rh_2]-[Pt_2]\}_n-$ depending on bridging ligands on the dirhodium complex. Although we have reported the structure of $[\{Rh_2(acam)_4\}\{Pt_2(piam)_2(NH_3)_4\}_2]_n(CF_3CO_2)_{4n}$ (**2′**),[32] further studies have not been initiated yet, because insufficient sample was obtained at that time. Here, we show two kinds of heterometallic 1D chains containing $[Rh_2(acam)_4]$, $[\{Rh_2(acam)_4\}\{Pt_2(piam)_2(NH_3)_4\}_2]_n(CF_3SO_3)_{4n}\cdot 2n$MeOH (**2**) and $[\{Rh_2(acam)_4\}\{Pt_2(piam)_2(NH_3)_4\}]_n(CF_3CO_2)_{2n}\cdot 2n$EtOH (**3**). Interestingly, **3** has unique metal repetitions, and we also discuss the metal−metal distances, oxidation states, and electronic structures of **1**−**3**.

Scheme 1. $[Rh_2(O_2CCH_3)_4]$ and $[Rh_2(acam)_4]$ with Schematic Electronic Structure

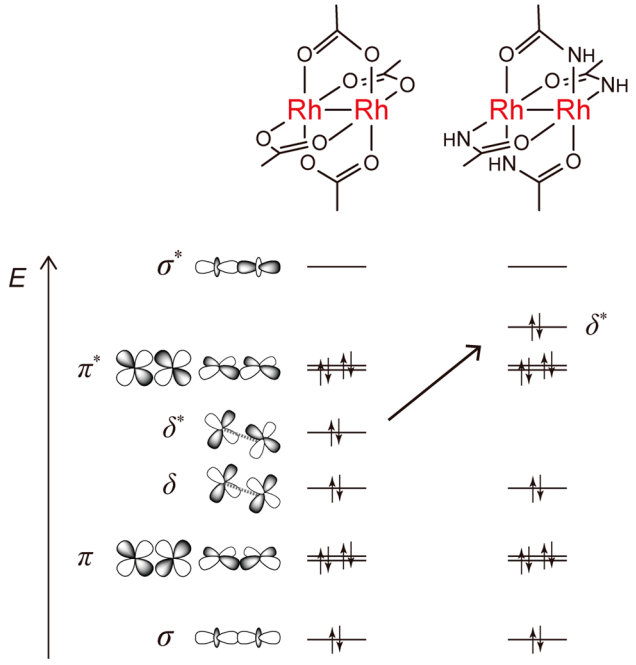

EXPERIMENTAL SECTION

Materials. Rhodium(III) chloride trihydrate and potassium tetrachloroplatinate(II) were obtained from Tanaka Kikinzoku Co. $AgCF_3CO_2$ and $AgCF_3SO_3$ were obtained from Aldrich Co. $NaCF_3CO_2$ was obtained from Wako Co. $NaCF_3SO_3$ was obtained from Tokyo Chemical Industry Co. *cis*-$[PtI_2(NH_3)_2]$,[37] *cis*-$[Pt(piam)_2(NH_3)_2]\cdot 2H_2O$,[38] and $[Rh_2(acam)_4]$[39,40] were synthesized according to the previous procedures. $[Rh_2(acam)_4]CF_3CO_2$ was prepared by a modification of method for preparing $[Rh_2(acam)_4(H_2O)_2]PF_6$.[41]

Synthesis of $[\{Rh_2(acam)_4\}\{Pt_2(piam)_2(NH_3)_4\}_2]_n(CF_3SO_3)_{4n}\cdot 2n$MeOH (2). An aqueous solution (2 mL) of *cis*-$[PtI_2(NH_3)_2]$ (0.19 g, 0.39 mmol) was stirred with 2 equiv of $AgCF_3SO_3$ (0.21 g, 0.82 mmol) overnight in the dark, and AgI was then removed by filtration. The colorless filtrate was stirred with 1 equiv of *cis*-$[Pt(piam)_2(NH_3)_2]\cdot 2H_2O$ (0.17 g, 0.37 mmol) and $NaCF_3SO_3$ (0.34 g, 2.0 mmol). The resulted dark-blue solution was cooled in the refrigerator to obtain crude sample of $[Pt_2(piam)_2(NH_3)_4](CF_3SO_3)_2$ (0.14 g) as dark-blue powder by the filtration. A small portion of the dark-blue powder (17 mg) and $[Rh_2(acam)_4]$ (4.0 mg, 9.1 μmol) were mixed in MeOH (3 mL), and the solution was slowly evaporated. After several days, yellow crystals with metallic luster were obtained (3.1 mg, 1.3 μmol). Yield 14% based on $[Rh_2(acam)_4]$. Anal. Calcd for $C_{34}H_{88}F_{12}N_{16}O_{22}Pt_4Rh_2S_4$: C, 16.91; H, 3.67; N, 9.28%. Found: C, 17.05; H, 3.70; N, 9.29%.

Synthesis of $[\{Rh_2(acam)_4\}\{Pt_2(piam)_2(NH_3)_4\}]_n(CF_3CO_2)_{2n}\cdot 2n$EtOH (3). An aqueous solution (6.2 mL) of *cis*-$[PtI_2(NH_3)_2]$ (0.30 g, 0.62 mmol) was stirred with 2 equiv of $AgCF_3CO_2$ (0.27 g, 1.22 mmol) overnight in the dark, and AgI was then removed by filtration. The colorless filtrate was stirred with 1 equiv of *cis*-$[Pt(piam)_2(NH_3)_2]\cdot 2H_2O$ (0.24 g, 0.52 mmol) overnight. The resulting dark-blue solution was evaporated to obtain dark-blue powder (0.44 g) that was a crude sample of $[Pt_2(piam)_2(NH_3)_4](CF_3CO_2)_2$. A small portion of the dark-blue powder (11 mg), $[Rh_2(acam)_4]$ (2.7 mg, 6.2 μmol), and $NaCF_3CO_2$ (8.2 mg, 60 μmol) were mixed in EtOH (3 mL), and the solution was slowly evaporated. After several days, brown crystals with metallic luster were obtained (3.5 mg, 2.5 μmol). Yield 43%. For elemental analysis these crystals were collected and dried in vacuo at room temperature for 24 h. Anal. Calcd for $C_{22}H_{48}F_6N_{10}O_{10}Pt_2Rh_2$: C, 19.98; H, 3.66; N, 10.59%. Found: C, 19.74; H, 3.70; N, 10.36%.

X-ray Structure Determination. Measurements were carried out on a Rigaku AFC7R diffractometer equipped with a normal focus Mo-target X-ray tube (λ = 0.710 70 Å) operated at 15 kW power (50 kV, 300 mA) and a Mercury CCD two-dimensional detector. A total of 744 frames were collected with a scan width of 0.5° with an exposure time of 10 s/frame. Empirical absorption correction[42] was performed for all data. The structures were solved by the direct method[43] with the subsequent difference Fourier syntheses and the refinement with the SHELX-97[44] operated by Yadokari-XG software package.[45] In both **2** and **3**, solvent molecules are refined without hydrogen atoms. Non-hydrogen atoms were refined anisotropically, and all hydrogen atoms were treated as riding atoms. The crystal data and structure refinement results are summarized in Table 1.

Table 1. Crystallographic Data and Structure Refinements for $[\{Rh_2(acam)_4\}\{Pt_2(piam)_2(NH_3)_4\}_2]_n(CF_3SO_3)_{4n}\cdot 2n$MeOH (2) and $[\{Rh_2(acam)_4\}\{Pt_2(piam)_2(NH_3)_4\}]_n(CF_3CO_2)_{2n}\cdot 2n$EtOH (3)

	2	3
empirical formula	$C_{34}H_{80}F_{12}N_{16}O_{22}Pt_4Rh_2S_4$	$C_{26}H_{48}F_6N_{10}O_{12}Pt_2Rh_2$
fw	2407.56	1402.74
cryst syst	triclinic	orthorhombic
space group	$P\bar{1}$	$P2_12_12_1$
a (Å)	11.235(3)	11.114(3)
b (Å)	13.045(3)	19.543(5)
c (Å)	14.126(4)	20.770(5)
α (deg)	74.317(11)	90
β (deg)	85.685(12)	90
γ (deg)	65.247(9)	90
V (Å^3)	1808.5(8)	4511.1(19)
Z	1	4
T (K)	123	123
D_c (Mg m^{-3})	2.211	2.065
abs coeff (mm^{-1})	8.371	6.988
F(000)	1146	2680
cryst size (mm^3)	0.20 × 0.10 × 0.05	0.25 × 0.10 × 0.05
measured reflns	14 525	36 719
indep reflns	8164 [R_{int} = 0.0530]	10 332 [R_{int} = 0.0978]
GOF on F^2	1.067	1.071
R [$I > 2\sigma(I)$]	R_1 = 0.0685, wR_2 = 0.1523	R_1 = 0.0725, wR_2 = 0.1529
R (all data)	R_1 = 0.0982, wR_2 = 0.1797	R_1 = 0.0924, wR_2 = 0.1668

dx.doi.org/10.1021/ic500305n | Inorg. Chem. 2014, 53, 4621−4628

Physical Measurements. The XPS measurements were carried out on a Quantera-SXM spectrometer at room temperature. Binding energies were measured relative to the C 1s peak (284.8 eV) of internal hydrocarbons. The UV−vis spectra were recorded on a Shimadzu UV-3100X spectrophotometer over the range from 260 to 1200 nm at room temperature. The diffuse reflectance spectra were recorded on a Hitachi U-4000 spectrophotometer over the range from 200 to 2500 nm at room temperature. Obtained reflectance spectra were converted to absorption spectra using the Kubelka−Munk function $F(R_\infty)$. The IR spectra were recorded on a PerkinElmer Spectrum 400 over the range from 400 to 2000 cm^{-1} at room temperature. X-band EPR spectra were measured on a JEOL JES-FA100 spectrometer. The field difference was calibrated by measuring the field intensity at the resonance of Mn^{2+}.

RESULTS AND DISCUSSION

Syntheses and Reaction in Solution. The previous procedure[32] for obtaining heterometallic 1D chains of $-\{[Pt_2]-[Rh_2]-[Pt_2]\}_n-$ containing $[Rh_2(acam)_4]$, $[\{Rh_2(acam)_4\}\{Pt_2(piam)_2(NH_3)_4\}_2]_n(CF_3CO_2)_{4n}$ (**2′**), was by slow evaporation of a MeOH solution containing $[Rh_2(acam)_4]$, $[Pt_2(piam)_2(NH_3)_4](CF_3CO_2)_2$, and $NaCF_3CO_2$ with the molar ratio of 1:2:20. We have also described a similar procedure in a MeCN solution containing $[Rh_2(acam)_4]$ and $[Pt_2(piam)_2(NH_3)_4](CF_3CO_2)_2$ with the ratio of 1:2 that afforded a few single crystals. Interaction of $[Rh_2(acam)_4]$ with $[Pt_2(piam)_2(NH_3)_4](CF_3CO_2)_2$ in MeCN was investigated with UV−vis spectroscopy. Figure 1a shows the UV−vis spectra of MeCN solutions of $[Rh_2(acam)_4]$ (0.1 mM) with various amounts of $[Pt_2(piam)_2(NH_3)_4](CF_3CO_2)_2$ in the ratio of 1:n (n = 0.5, 1, 1.5, ..., 4). The absorbance spectrum of $[Rh_2(acam)_4]$ (n = 0) exhibits two bands, 350 and 500 nm, attributed to $\pi^*(Rh_2) \rightarrow \sigma^*(Rh-O)$ and $\pi^*(Rh_2) \rightarrow \sigma^*(Rh_2)$ transitions in the Rh_2 core,[46,47] respectively. Three new bands, at 322, 456, and around 1034 nm, intensify as the concentration of $[Pt_2(piam)_2(NH_3)_4](CF_3CO_2)_2$ increases. The two bands around 456 and 1034 nm can be assigned to $\pi^*(Rh_2) \rightarrow \sigma^*(Rh_2)$ and $\delta\ (Rh_2) \rightarrow \delta^*\ (Rh_2)$ of $[Rh_2(acam)_4]^+$,[46] respectively, which indicates that the addition of $[Pt_2(piam)_2(NH_3)_4](CF_3CO_2)_2$ enhances the oxidation of $[Rh_2(acam)_4]$. On the basis of the absorbance at 1034 nm for $[Rh_2(acam)_4]CF_3CO_2$, the ratio of $[Rh_2(acam)_4]^+/[Rh_2(acam)_4]$ can be calculated to obtain 5, 7, 11, ..., 26% at n = 0.5, 1, 1.5, ..., 4, respectively, where the oxidation is linearly enhanced.

In contrast, Figure 1b shows the UV−vis spectra of $[Rh_2(acam)_4]CF_3CO_2$ (0.1 mM) and various amounts of $[Pt_2(piam)_2(NH_3)_4](CF_3CO_2)_2$ with the ratio of 1:n (n = 0.5, 1, 1.5, ..., 4) in MeCN. Because the absorbance values of the $\delta\ (Rh_2) \rightarrow \delta^*\ (Rh_2)$ bands around 1034 nm are constant for all the solutions, the concentration of $[Rh_2(acam)_4]^+$ does not change. As the concentration of $[Pt_2(piam)_2(NH_3)_4](CF_3CO_2)_2$ increases, the bands around 330 and 480 nm grow, implying that $[Rh_2(acam)_4]CF_3CO_2$ interacts with $[Pt_2(piam)_2(NH_3)_4](CF_3CO_2)_2$ to afford new species. The appearance of the band around 330 nm is the result of the filled σ-type orbital → vacant σ-type orbital, which is attributed to the formation of unbridged Rh−Pt bonds.[34] Thus, the results in Figure 1 imply that both $[Rh_2(acam)_4]$ and $[Rh_2(acam)_4]^+$ interact with $[Pt_2(piam)_2(NH_3)_4](CF_3CO_2)_2$. However, in the mixture of $[Rh_2(acam)_4]$ and $[Pt_2(piam)_2(NH_3)_4](CF_3CO_2)_2$, the oxidation of $[Rh_2(acam)_4]$ as a side reaction complicates the system, which was one of the reasons for the low yield of this system. Subsequently, we have screened the reaction conditions with various counteranions and solvents, and succeeded in obtaining two kinds of single crystals, $[\{Rh_2(acam)_4\}\{Pt_2(piam)_2(NH_3)_4\}_2]_n(CF_3SO_3)_{4n}\cdot 2n$MeOH (**2**) and $[\{Rh_2(acam)_4\}\{Pt_2(piam)_2(NH_3)_4\}]_n(CF_3CO_2)_{2n}\cdot 2n$EtOH (**3**), with better yields.

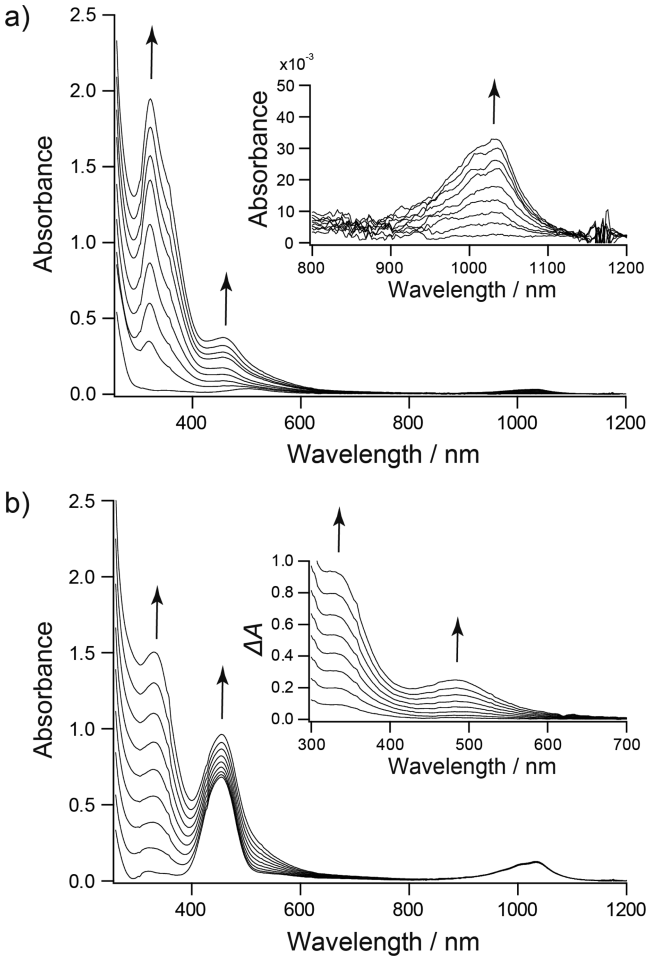

Figure 1. UV−vis spectra of 0.1 mM solution of (a) $[Rh_2(acam)_4]$ and (b) $[Rh_2(acam)_4]CF_3CO_2$ in MeCN containing 0−4 equiv of $[Pt_2(piam)_2(NH_3)_4](CF_3CO_2)_2$ at room temperature. Inset in b: Difference spectra of each concentration of $[Pt_2(piam)_2(NH_3)_4](CF_3CO_2)_2$ solution from a solution containing 0.1 mM $[Rh_2(acam)_4]^+$.

Crystal Structure of $[\{Rh_2(acam)_4\}\{Pt_2(piam)_2(NH_3)_4\}_2]_n(CF_3SO_3)_{4n}\cdot 2n$MeOH (2). Figure 2 shows the crystal structure of **2**. The paddlewheel dinuclear complexes of (2,2)-*cis*-$[Rh_2(acam)_4]$ are sandwiched by $[Pt_2(piam)_2(NH_3)_4]$ at both ends with metal−metal bonds to form hexanuclear $[Pt_2]-[Rh_2]-[Pt_2]$ units, where a crystallographic inversion center lies at the center of the rhodium complex (Figure 2a). The platinum atoms in $[Pt_2]$ complexes are bonded to a rhodium complex with a bond distance of Rh(1)−Pt(2) = 2.7624(11) Å and a torsion angle L_{eq}−Rh−Pt−N of about 41−44° (Figure 2b). The hexanuclear $[Pt_2]-[Rh_2]-[Pt_2]$ segments are linked by hydrogen bonds with a Pt(1)−Pt(1″) distance of 3.0786(12) Å, resulting in the formation of a quasi-1D infinite chain, expressed as $-\{[Rh_2]-[Pt_2]-[Pt_2]\}_n-$, where the linked platinum dinuclear complexes form a tetranuclear platinum backbone $[Pt_2]-[Pt_2]$, similar to "platinum blue" compounds.[48,49]

dx.doi.org/10.1021/ic500305n | Inorg. Chem. 2014, 53, 4621−4628

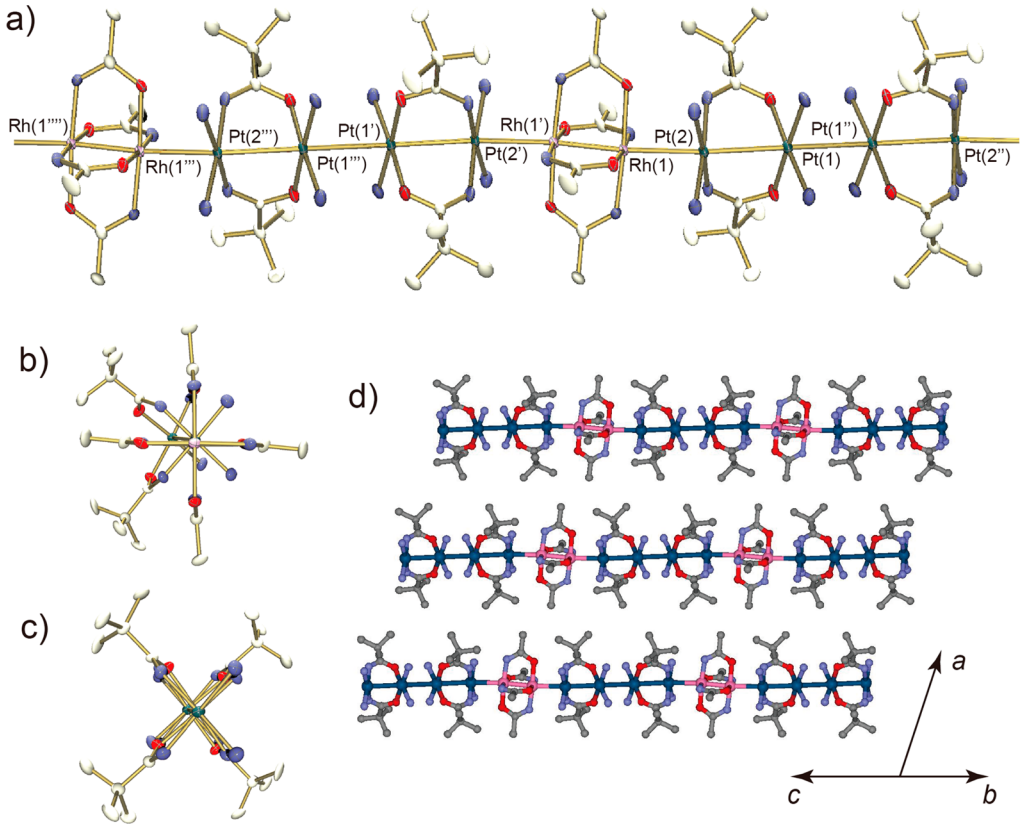

Figure 2. Crystal structures of (a) $[\{Rh_2(acam)_4\}\{Pt_2(piam)_2(NH_3)_4\}_2]_n(CF_3SO_3)_{4n}\cdot 2n$MeOH (**2**). Stacking fashions between (b) $[Rh_2]$ and $[Pt_2]$, or (c) $[Pt_2]$ and $[Pt_2]$. (d) Crystal packing of the 1D chains in **2**. The hydrogen atoms, anions, and solvent molecules are omitted for clarity.

Multiple hydrogen bonds between ligands support the unbridged metal−metal bonds. Between $[Pt_2]$ and $[Pt_2]$, the complexes are stacked in a face-to-face fashion (Figure 2c), which is induced by quadruple hydrogen bonds between the oxygen atoms of the piam groups and the nitrogen atoms of the amine ligands, indicating that $[Pt_2]$ is a HH (head−head)-typed complex having the same coordination direction of piam ligands (Scheme 2). Consequently, between $[Rh_2]$ and $[Pt_2]$, all four atoms are hydrogen bond donors in the platinum part, whereas there are two acceptors and two donors in the rhodium part. Although the rhodium part has a small number of hydrogen bond acceptor sites such that both attraction and repulsion forces coexist between the $[Rh_2]$ and $[Pt_2]$ units, two hydrogen bonds between the amidate oxygen atoms in the $[Rh_2]$ and the amine ligands in the $[Pt_2]$ are effectively formed with O−N distances of 2.96 and 3.05 Å. The dihedral angle between the Pt and Rh coordination planes is 6.6°, which results from the hydrogen bonds between amine and oxygen atoms in the acam ligand. Additional hydrogen bonds are formed between amine ligands, $CF_3SO_3^-$ ions, and accommodated MeOH molecules (Supporting Information Figure S3), where $CF_3SO_3^-$ ions bridge 1D chains. As shown in Figure 2d, each chain is aligned in a parallel fashion in the crystal.

Scheme 2. Hydrogen Bonds between Dinuclear Complexes in 2 and 3

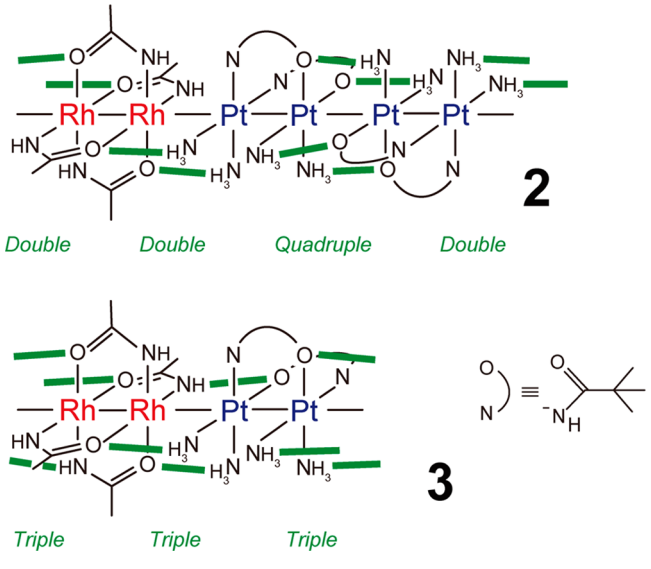

Crystal Structure of $[\{Rh_2(acam)_4\}\{Pt_2(piam)_2(NH_3)_4\}]_n\cdot(CF_3CO_2)_{2n}\cdot 2n$EtOH (3). Figure 3 shows the crystal structure of **3**. The paddlewheel dinuclear complexes of (2,2)-*cis*-$[Rh_2(acam)_4]$ are sandwiched by $[Pt_2(piam)_2(NH_3)_4]$ at both ends with metal−metal bonds having Pt(1′)−Rh(2) bond distances of 2.7641(14) Å and Pt(2)−Rh(1) bond distances of 2.7894(14) Å (Figure 3a). The chain structure is distinct from **2**, where both platinum atoms in $[Pt_2(piam)_2(NH_3)_4]$ are bonded to $[Rh_2(acam)_4]$ to form a 1D infinite chain expressed as $-\{[Rh_2]-[Pt_2]\}_n-$. As shown in Figure 3b,c, two kinds of complexes, $[Rh_2]$ and $[Pt_2]$, are stacked in a staggered fashion. Although the coordination planes of Rh and Pt atoms are almost parallel with dihedral angles of 0.7° and 2.2°, the chain is wavy, and originates from the large dihedral angle (34.1°) between two Pt coordination planes in the half-lantern fashion

dx.doi.org/10.1021/ic500305n | Inorg. Chem. 2014, 53, 4621−4628

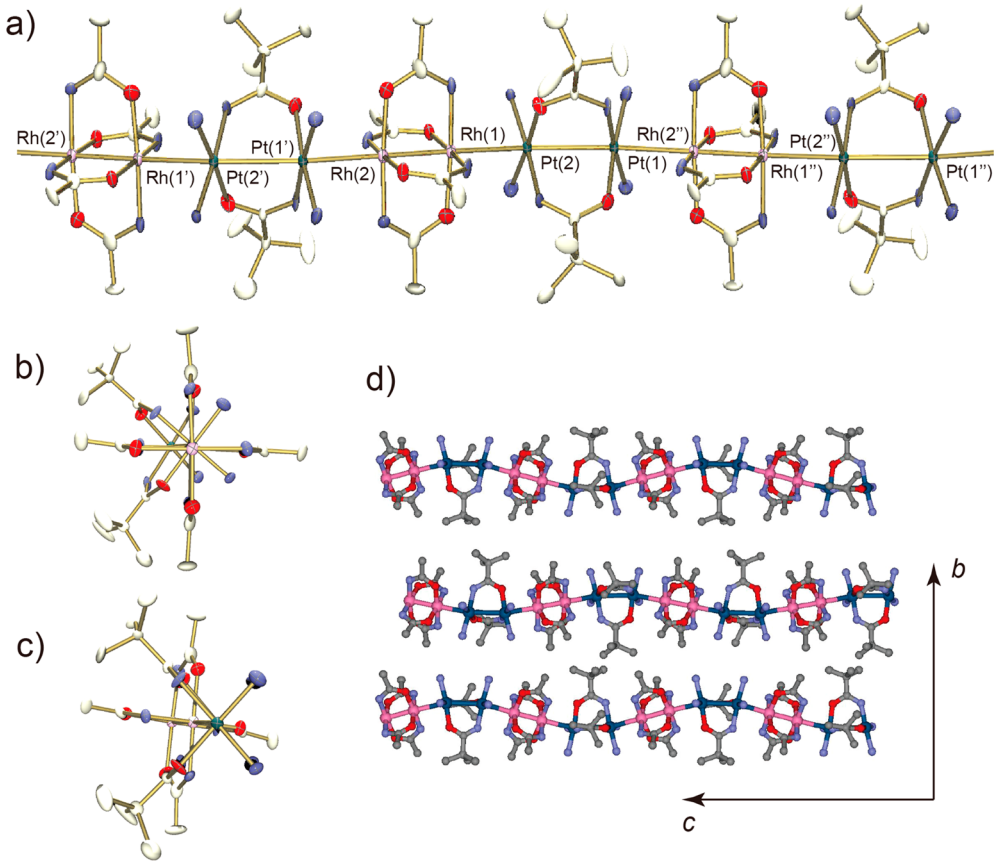

Figure 3. Crystal structures of (a) $[\{Rh_2(acam)_4\}\{Pt_2(piam)_2(NH_3)_4\}]_n(CF_3CO_2)_{2n}{\cdot}2n$EtOH (**3**). Stacking fashions between $[Rh_2]$ and $[Pt_2]$ from perspective of (b) $[Rh_2]$ or (c) $[Pt_2]$. (d) Crystal packing of the 1D chains in **3**. The hydrogen atoms, anions, and solvent molecules are omitted for clarity.

Table 2. Comparison of Selected Bond Distances (Å) between 1, 2, 3, and Reported Compounds

compd	Rh−Rh	Rh−Pt	intra Pt−Pt	intra Pt−Pt	ref
$[Rh_2(acam)_4(H_2O)_2]$	2.415(1)				39
$[Rh_2(acam)_4(H_2O)_2]^+$	2.4084(10)				41
$[Pt_4^{II,II,II,II}(piam)_4(NH_3)_8]^{4+}$			2.9546(11)	3.1256(12)	23
$[Pt_4^{II,II,II,III}(piam)_4(NH_3)_8]^{5+}$			2.8039(9)	2.8603(12)	23
1	2.3832(17)	2.7460(10)	2.9376(7)	3.0893(9)	32
2	2.4205(18)	2.7624(11)	2.9033(9)	3.0786(12)	this work
2′	2.423(2)	2.7781(14)	2.9299(9)	3.0651(12)	32
3	2.4095(16)	2.7641(14), 2.7894(14)	2.9332(9)		this work

of $[Pt_2]$. All chains extend along the *c* axis in parallel (Figure 3d).

The HH and HT isomerization in half-lantern-typed $[Pt_2^{II,II}]$ complexes are generally occurring in solution.[50,51] In **3**, the most accurate X-ray analyses indicate that $[Pt_2]$ is a HT-type complex having the opposite coordination direction of piam ligands. Consequently, between $[Rh_2]$ and $[Pt_2]$, there are three hydrogen bond donors and one acceptor site in the platinum part, whereas two donors and two acceptors occur in the rhodium part, such that three hydrogen bonds with N−*O* = 3.0−3.2 Å are formed between the $[Rh_2]$ and $[Pt_2]$ units (Scheme 2). The amine ligands coordinated to Pt atoms are hydrogen bonded to both $CF_3CO_2^-$ ions and accommodated EtOH molecules (Supporting Information Figure S4), whereas the piam and acam ligands only play a role in hydrogen bonding to each other. It could be considered that this HH and HT isomerization also lowered the yield of complexes with $[Rh_2(acam)_4]$, and the oxidation of $[Rh_2(acam)_4]$ as a side reaction.

Comparison of Crystal Structures and Metal Oxidation States in 2 and 3. The sum of metal oxidation states for the $[Pt_2]-[Rh_2]-[Pt_2]$ hexameric segment in **2** is +12, which was determined from the number of $CF_3SO_3^-$ ions per hexameric unit in the X-ray structure refinement. In **3**, the sum of metal oxidation states of +8 for the $[Rh_2]-[Pt_2]$ tetrameric segment was deduced from the two $CF_3CO_2^-$ ions per the tetrameric segment. Table 2 summarizes the metal−metal distances of **1**−**3** and their related compounds. The Rh−Rh bond distances of the paddlewheel dirhodium parts in **2** (2.4205(18) Å) and **3** (2.4095(16) Å) are longer than those distances found in **1** (2.3832(17) Å), which is attributed to the ligand characters. The Pt−Pt bond distance reflects the oxidation state of the platinum atoms.[48,49] In **2**, both the Pt−Pt bond distance of the intraunit (Pt(1)−Pt(2) = 2.9033(9) Å)

dx.doi.org/10.1021/ic500305n | Inorg. Chem. 2014, 53, 4621−4628

and the interunit (Pt(1″)−Pt(1) = 3.0786(12) Å) distances are shorter than those of $[Pt_4^{II,II,II,II}(piam)_4(NH_3)_8](PF_6)_4\cdot 2H_2O$ (intraunit = 2.9546(11) Å, interunit = 3.1256(12) Å) and longer than those of $[Pt_4^{II,II,II,III}(piam)_4(NH_3)_8](PF_6)_4(ClO_4)\cdot 2H_2O$ (intradimer = 2.8039(9) Å, interdimer = 2.8603(12) Å).[23] By contrast, in **3**, the Pt−Pt bond distance is obviously closer to that in $[Pt_4^{II,II,II,II}(piam)_4(NH_3)_8](PF_6)_4\cdot 2H_2O$.

To assign oxidation states to each metal atom in **2** and **3**, XPS measurements were conducted (Figure 4). As shown in Figure 4c,d, the $3d_{3/2}$ signals of Rh overlap the Pt $4d_{5/2}$ signals. The Rh $3d_{5/2}$ binding energies were 308.2 (**2**) and 308.0 (**3**) eV, which are closer to the value for $[Rh_2^{II,II}(acam)_4]$ (308.1 eV, Figure 4a) than that for $[Rh_2^{II,III}(acam)_4]CF_3CO_2$ (308.9 eV, Figure 4b). However, the Pt $4f_{7/2}$ binding energies for **2** and **3** were determined to be 73.1 and 72.9 eV, respectively, which are closer to those of $[Pt_2^{II,II}(piam)_2(NH_3)_4](PF_6)_2$ (73.2 eV) and $[Pt_2^{II,II}(en)_2(\alpha\text{-pyridonato})_2](NO_3)_2$ (73.1 eV; en = ethylenediamine)[52] than to that of $[Pt_2^{III,III}(NH_3)_4(\alpha\text{-pyrrolidonato})_2(NO_3)_2](NO_3)_2$ (74.6 eV).[52] Consequently, the formal oxidation states of **2** and **3** are $-\{[Rh_2^{II,II}]-[Pt_2^{II,II}]-[Pt_2^{II,II}]\}_n-$ and $-\{[Rh_2^{II,II}]-[Pt_2^{II,II}]\}_n-$, respectively, which are unchanged from those in the starting compounds.

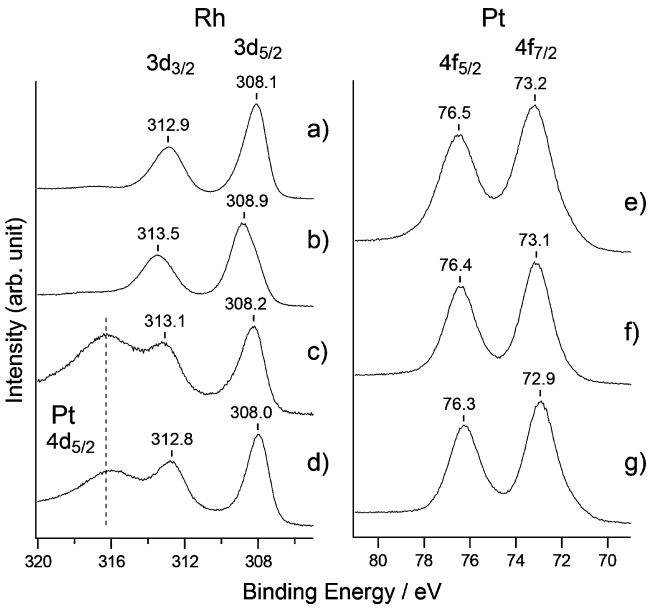

Figure 4. Rh $3d_{3/2}$ and $3d_{5/2}$ (left) and Pt $4f_{5/2}$ and $4f_{7/2}$ (right) core levels of XPS for (a) $[Rh_2(acam)_4]$, (b) $[Rh_2(acam)_4]CF_3CO_2$, (c) **2**, (d) **3**, (e) $[Pt_2(piam)_2(NH_3)_4](PF_6)_2$, (f) **2**, (g) **3**.

Electronic Structures of 2 and 3. Figure 5 shows the simple molecular orbital diagram of the hexanuclear complex aligned as $[Pt_2^{II,II}]-[Rh_2^{II,II}]-[Pt_2^{II,II}]$ or tetranuclear complex aligned as $[Rh_2^{II,II}]-[Pt_2^{II,II}]$. The diagram represents the sequence of six or four molecular orbitals made from all possible combinations of the metal σ orbitals, where energy increases with the number of nodes along the chain direction.[53] As reported previously,[34] the DFT calculation for these kinds of 1D complexes containing $Pt^{II}-Rh^{II}$ bonds showed that the LUMO consists of σ-type orbitals ($\sigma^*(Pt_2)-\sigma^*(Rh_2)-\sigma^*(Pt_2)$ or $\sigma^*(Rh_2)-\sigma^*(Pt_2)$) that have all antibonding combinations of $\sigma^*(Pt_2)$ and $\sigma^*(Rh_2)$, and other stabilized filled σ-type orbitals were also found. The calculation also showed that π-type orbitals in $[Rh_2]$ are essentially mixed with the π orbitals of the piam ligands through d orbitals in platinum parts.[34] In this case, because the ligands of $[Rh_2]$ in both **2** and **3** are amidate ligands, δ^* orbitals in $[Rh_2]$ are destabilized. Therefore, the HOMOs in both **2** and **3** are expected to be δ^* orbitals in $[Rh_2]$ or mixed π-type orbitals.

Figure 6 shows the diffuse reflectance spectra of **1**−**3**, $[Rh_2(acam)_4]$, and $[Rh_2(acam)_4]CF_3CO_2$. In **1**−**3**, three characteristic bands labeled E_1, E_2, and E_3 are observed, where the larger peak of E_1 is attributed to transition filled σ-type orbitals ($\sigma^*(Pt_2)-\sigma(Rh_2)-\sigma^*(Pt_2)$) to LUMO, while E_2 and E_3 are attributed to orbitals including $\pi^*(Rh_2)$ to LUMO.[34] The spectrum of **2** shows four peaks at 2.90 (E_1), 1.80 (E_2), 1.52 (E_3), and 1.19 eV (Figure 6b) instead of those around 2.10 eV in $[Rh_2(acam)_4]$ attributed to $\pi^*(Rh_2) \rightarrow \sigma^*(Rh_2)$

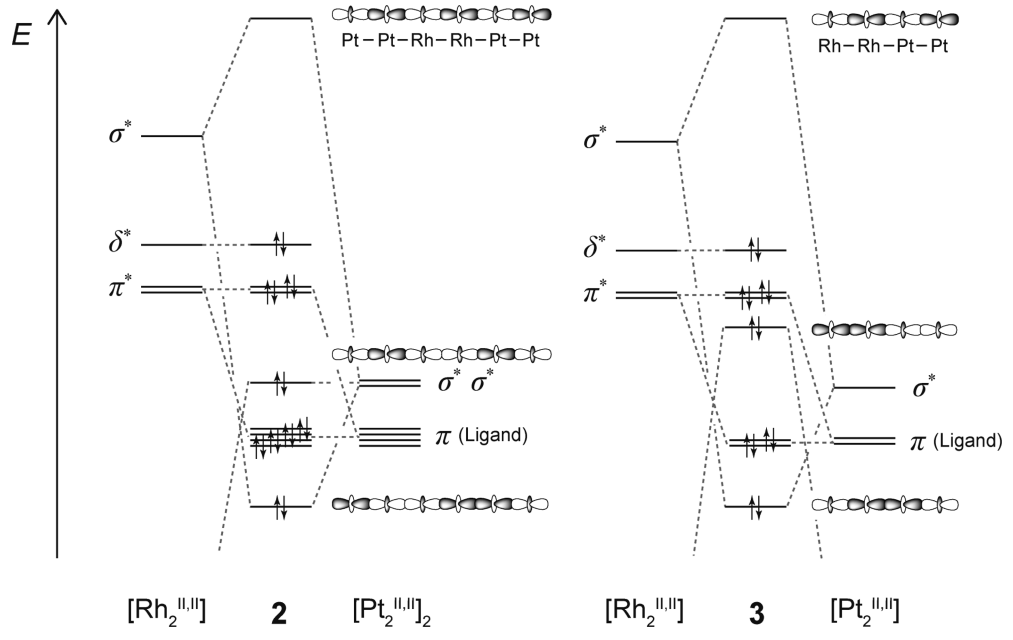

Figure 5. Schematic molecular orbital diagrams of $[\{Rh_2(acam)_4\}\{Pt_2(piam)_2(NH_3)_4\}_2]^{4+}$ (left) and $[\{Rh_2(acam)_4\}\{Pt_2(piam)_2(NH_3)_4\}]^{2+}$ (right).

dx.doi.org/10.1021/ic500305n | Inorg. Chem. 2014, 53, 4621−4628

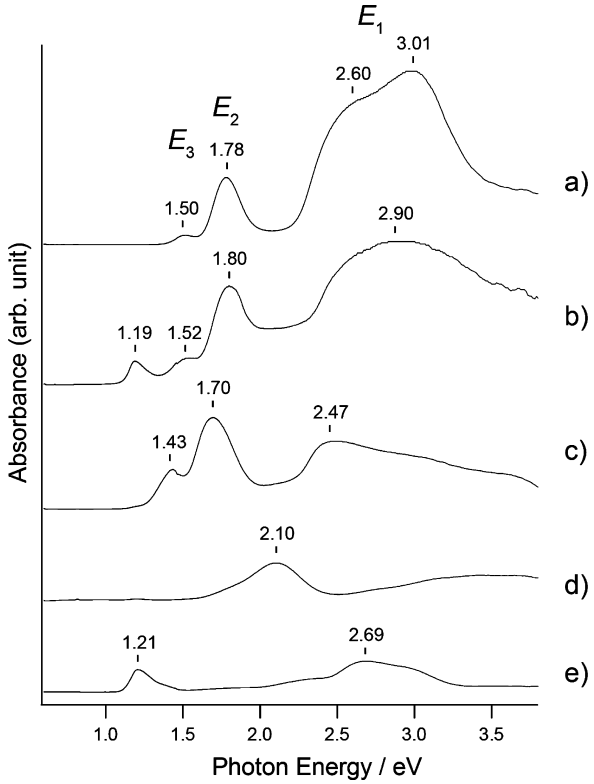

Figure 6. Diffuse reflectance spectra of (a) **1**, (b) **2**, (c) **3**, (d) $[Rh_2(acam)_4]$, and (e) $[Rh_2(acam)_4]CF_3CO_2$ with MgO at room temperature.

transitions in the Rh_2 core (Figure 6d).[46,47] Considering that both **1** and **2** have the same $-\{[Rh_2]-[Pt_2]-[Pt_2]\}_n-$ metal repeating units, it is reasonable to observe similar bands E_1, E_2, and E_3. However, an additional band at 1.19 eV is also observed in **2**, which is close to the band at 1.21 eV in $[Rh_2(acam)_4]$-CF_3CO_2 attributed to δ $(Rh_2) \rightarrow \delta^*$ (Rh_2) (Figure 6e).[46] By contrast, in **3**, all peaks, E_1, E_2, and E_3, are lower than the corresponding peaks in **1** and **2**. In particular, E_1 (2.47 eV) in **3** is about 0.4 eV lower than in **2**, indicating that the gap between filled and vacant σ-type orbitals is narrower in **3**. The reason is probably the result of the higher destabilized filled σ-type orbital which is composed of antibonding orbital between $\sigma(Rh_2)$ and $\sigma(Pt_2)$ (Figure 5 right), where the peak of E_1 in **3** is attributed to transition $\sigma(Rh_2)-\sigma(Pt_2)$ to $\sigma^*(Rh_2)-\sigma^*(Pt_2)$.

As mentioned above, **2** and **3** have $-\{[Rh_2^{II,II}]-[Pt_2^{II,II}]-[Pt_2^{II,II}]\}_n-$ and $-\{[Rh_2^{II,II}]-[Pt_2^{II,II}]\}_n-$ oxidation states, respectively, being diamagnetic. However, for powder samples of both **2** and **3**, electron paramagnetic resonance (EPR) spectra were recorded at 77 K. As shown in Supporting Information Figure S6, the spectra of **2** and **3** show axial-type signals of $g_\perp = 2.105$ and $g_\parallel = 1.929$, $g_\perp = 2.105$ and $g_\parallel = 1.933$, respectively, showing triple splitting of the $g_\parallel$ with $A_\parallel = 22 \times 10^{-4}$ cm^{-1} and $A_\parallel = 24 \times 10^{-4}$ cm^{-1}, respectively. Taking into account that those spectral profiles are similar to that for $[Rh_2(acam)_4]^+$,[36] the observed spins lie in the δ^* orbitals of $[Rh_2]$. Although the powder samples of both **2** and **3** were prepared from each single crystal, the possibility of impurity $[Rh_2(acam)_4]^+$ cannot be discarded. However, if both compounds are partially oxidized, taking advantage of weighted DPPH as the standard sample, we estimated the spin concentrations of 6.8×10^{-7} (**2**) and 6.1×10^{-7} (**3**) mol/g; that is, one unpaired electron exits approximately per four and five thousand metal atoms, respectively.

CONCLUSION

In this work, we have succeeded in obtaining two kinds of novel 1D chains composed of metal−metal bonds containing $[Rh_2(acam)_4]$ and $[Pt_2(piam)_2(NH_3)_4]$, where different metal repeating units, $-\{[Rh_2]-[Pt_2]-[Pt_2]\}_n-$ and $-\{[Rh_2]-[Pt_2]\}_n-$, have been achieved taking advantage of different isomers of $[Pt_2]$ complex. The XPS and diffuse reflectance spectra revealed that all the metal oxidation states in both **2** and **3** are +2, which are not changed from the starting materials. Compound **2** has a similar metal repeating sequence to **1**, $-\{[Rh_2]-[Pt_2]-[Pt_2]\}_n-$, where only the bridging ligands in $[Rh_2]$ are different, namely acetate and acetamidate, leading to the modulation of HOMO, π^*, and δ^* orbitals. In **3**, each $[Rh_2(acam)_4]$ is linked by two platinum atoms, where the diffuse reflectance spectra revealed that the gap between filled and vacant σ-type orbitals is narrower than **2**. It may be possible to remove electrons from the δ^* in the $[Rh_2]$ part, taking into account that the 1D backbones are mainly constructed from the σ- or π-character orbitals. We are now trying to synthesize 1D chains with mixed valence by the oxidation of $[Rh_2]$.

ASSOCIATED CONTENT

Supporting Information

Detailed crystal structures, UV−vis spectra, IR spectra, EPR spectra, and crystal information files (CIF). This material is available free of charge via the Internet at http://pubs.acs.org.

AUTHOR INFORMATION

Corresponding Author

*E-mail: k_uemura@gifu-u.ac.jp.

Notes

The authors declare no competing financial interest.

ACKNOWLEDGMENTS

This work was supported by the Grants-in-Aid for Scientific Research (Scientific Research (C) 24550074) and Kurata Memorial Hitachi Science and Technology Foundation.

REFERENCES

(1) Miller, J. S. *Extended Linear Chain Compounds, Vol 1−3*; Plenum: New York, 1982.
(2) Kitagawa, H.; Mitani, T. *Coord. Chem. Rev.* **1999**, *190−192*, 1169−1184.
(3) Bera, J. K.; Dunbar, K. R. *Angew. Chem., Int. Ed.* **2002**, *41*, 4453−4457.
(4) Yamashita, M.; Takaishi, S. *Bull. Chem. Soc. Jpn.* **2006**, *79*, 1820−1833.
(5) Mashima, K. *Bull. Chem. Soc. Jpn.* **2010**, *83*, 299−312.
(6) Givaja, G.; Amo-Ochoa, P.; Gómez-García, C. J.; Zamora, F. *Chem. Soc. Rev.* **2012**, *41*, 115−147.
(7) Finniss, G. M.; Canadell, E.; Campana, C.; Dunbar, K. R. *Angew. Chem., Int. Ed.* **1996**, *35*, 2772−2774.
(8) Prater, M. E.; Pence, L. E.; Clerac, R.; Finniss, G. M.; Campana, C.; Auban-Senzier, P.; Jerome, D.; Canadell, E.; Dunbar, K. R. *J. Am. Chem. Soc.* **1999**, *121*, 8005−8016.
(9) Cotton, F. A.; Dikarev, E. V.; Petrukhina, M. A. *J. Chem. Soc., Dalton Trans.* **2000**, 4241−4243.
(10) Pruchnik, F. P.; Jakimowicz, P.; Ciunik, Z.; Stanislawek, K.; Oro, L. A.; Tejel, C.; Ciriano, M. A. *Inorg. Chem. Commun.* **2001**, *4*, 19−22.

(11) Mitsumi, M.; Goto, H.; Umebayashi, S.; Ozawa, Y.; Kobayashi, M.; Yokoyama, T.; Tanaka, H.; Kuroda, S.-i.; Toriumi, K. *Angew. Chem., Int. Ed.* **2005**, *44*, 4164−4168.
(12) Campbell, M. G.; Powers, D. C.; Raynaud, J.; Graham, M. J.; Xie, P.; Lee, E.; Ritter, T. *Nat. Chem.* **2011**, *3*, 949−953.
(13) Campbell, M. G.; Zheng, S.-L.; Ritter, T. *Inorg. Chem.* **2013**, *52*, 13295−13297.
(14) Sakai, K.; Ishigami, E.; Konno, Y.; Kajiwara, T.; Ito, T. *J. Am. Chem. Soc.* **2002**, *124*, 12088−12089.
(15) Mitsumi, M.; Ueda, H.; Furukawa, K.; Ozawa, Y.; Toriumi, K.; Kurmoo, M. *J. Am. Chem. Soc.* **2008**, *130*, 14102−14104.
(16) Guijarro, A.; Castillo, O.; Calzolari, A.; Miguel, P. J. S.; Gómez-García, C. J.; Felice, R. d.; Zamora, F. *Inorg. Chem.* **2008**, *47*, 9736−9738.
(17) Kitagawa, H.; Onodera, N.; Sonoyama, T.; Yamamoto, M.; Fukawa, T.; Mitani, T.; Seto, M.; Maeda, Y. *J. Am. Chem. Soc.* **1999**, *121*, 10068−10080.
(18) Mitsumi, M.; Murase, T.; Kishida, H.; Yoshinari, T.; Ozawa, Y.; Toriumi, K.; Sonoyama, T.; Kitagawa, H.; Mitani, T. *J. Am. Chem. Soc.* **2001**, *123*, 11179−11192.
(19) Yamashita, M.; Kawakami, D.; Matsunaga, S.; Nakayama, Y.; Sasaki, M.; Takaishi, S.; Iwahori, F.; Miyasaka, H.; Sugiura, K.; Wada, Y.; Miyamae, H.; Matsuzaki, H.; Okamoto, H.; Tanaka, H.; Marumoto, K.; Kuroda, S. *Angew. Chem., Int. Ed.* **2004**, *43*, 4763−4767.
(20) Takaishi, S.; Kawakami, D.; Yamashita, M.; Sasaki, M.; Kajiwara, T.; Miyasaka, H.; Sugiura, K.-i.; Wakabayashi, Y.; Sawa, H.; Matsuzaki, H.; Kishida, H.; Okamoto, H.; Watanabe, H.; Tanaka, H.; Marumoto, K.; Ito, H.; Kuroda, S.-i. *J. Am. Chem. Soc.* **2006**, *128*, 6420−6425.
(21) Kobayashi, A.; Kojima, T.; Ikeda, R.; Kitagawa, H. *Inorg. Chem.* **2006**, *45*, 322−327.
(22) Mitsumi, M.; Yoshida, Y.; Kohyama, A.; Kitagawa, Y.; Ozawa, Y.; Kobayashi, M.; Toriumi, K.; Tadokoro, M.; Ikeda, N.; Okumura, M.; Kurmoo, M. *Inorg. Chem.* **2009**, *48*, 6680−6691.
(23) Uemura, K.; Fukui, K.; Nishikawa, H.; Arai, S.; Matsumoto, K.; Oshio, H. *Angew. Chem., Int. Ed.* **2005**, *44*, 5459−5464.
(24) Uemura, K.; Fukui, K.; Yamasaki, K.; Matsumoto, K.; Ebihara, M. *Inorg. Chem.* **2010**, *49*, 7323−7330.
(25) Erxleben, A.; Lippert, B. *J. Chem. Soc., Dalton Trans.* **1996**, 2329−2333.
(26) Yamaguchi, T.; Yamazaki, F.; Ito, T. *J. Am. Chem. Soc.* **2001**, *123*, 743−744.
(27) Chen, W.; Liu, F.; Matsumoto, K.; Autschbach, J.; Guennic, B. L.; Ziegler, T.; Maliarik, M.; Glaser, J. *Inorg. Chem.* **2006**, *45*, 4526−4536.
(28) Chen, W.; Liu, F.; Xu, D.; Matsumoto, K.; Kishi, S.; Kato, M. *Inorg. Chem.* **2006**, *45*, 5552−5560.
(29) Hayoun, R.; Zhong, D. K.; Rheingold, A. L.; Doerrer, L. H. *Inorg. Chem.* **2006**, *45*, 6120−6122.
(30) Doerrer, L. H. *Dalton Trans.* **2010**, *39*, 3543−3553.
(31) Givaja, G.; Castillo, O.; Mateo, E.; Gallego, A.; Gómez-García, C. J.; Calzolari, A.; Felice, R. d.; Zamora, F. *Chem.—Eur. J.* **2012**, *18*, 15476−15484.
(32) Uemura, K.; Ebihara, M. *Inorg. Chem.* **2011**, *50*, 7919−7921.
(33) Uemura, K.; Sakurai, K.; Yasuda, E.; Ebihara, M. *Polyhedron* **2012**, *45*, 35−42.
(34) Uemura, K.; Ebihara, M. *Inorg. Chem.* **2013**, *52*, 5535−5550.
(35) Hereafter, we omit the expression of (2,2)-*cis*- for clarity.
(36) Kawamura, T.; Katayama, H.; Nishikawa, H.; Yamabe, T. *J. Am. Chem. Soc.* **1989**, *111*, 8156−8160.
(37) Dkhara, S. C. *Indian J. Chem.* **1970**, *8*, 193−194.
(38) Chen, W.; Matsumoto, K. *Inorg. Chim. Acta* **2003**, *342*, 88−96.
(39) Ahsan, M. Q.; Bernal, I.; Bear, J. L. *Inorg. Chem.* **1986**, *25*, 260−265.
(40) Doyle, M. P.; Bagheri, V.; Wandless, T. J.; Harn, N. K.; Brinker, D. A.; Eagle, C. T.; Loh, K.-L. *J. Am. Chem. Soc.* **1990**, *112*, 1906−1912.
(41) Ebihara, M.; Fuma, Y. *Acta Crystallogr.* **2006**, *C62*, m284−m289.
(42) *Rigaku, REQAB. Version 1.1*; Rigaku Corporation: Tokyo, Japan, 1998.
(43) Altomare, A.; Burla, M. C.; Camalli, M.; Cascarano, G. L.; Giacovazzo, C.; Guagliardi, A.; Moliterni, A. G. G.; Polidori, G.; Spagna, R. *J. Appl. Crystallogr.* **1999**, *32*, 115−119.
(44) Sheldrick, G. M. *Acta Crystallogr.* **2008**, *A64*, 112−122.
(45) Yadokari-XG, Software for Crystal Structure Analyses, Wakita K. 2001; Release of Software (Yadokari-XG 2009) for Crystal Structure Analyses: Kabuto, C.; Akine, S.; Nemoto, T.; Kwon, E. *J. Cryst. Soc. Jpn.* **2009**, *51*, 218−224.
(46) Kadish, K. M.; Lançon, D.; Dennis, A. M.; Bear, J. L. *Inorg. Chem.* **1982**, *21*, 2987−2992.
(47) Zhu, T. P.; Ahsan, M. Q.; Malinski, T.; Kadish, K. M.; Bear, J. L. *Inorg. Chem.* **1984**, *23*, 2−3.
(48) Barton, J. K.; Rabinowitz, H. N.; Szalda, D. J.; Lippard, S. J. *J. Am. Chem. Soc.* **1977**, *99*, 2827−2829.
(49) Barton, J. K.; Szalda, D. J.; Rabinowitz, H. N.; Waszczak, J. V.; Lippard, S. J. *J. Am. Chem. Soc.* **1979**, *101*, 1434−1441.
(50) O'Halloran, T. V.; Lippard, S. J. *J. Am. Chem. Soc.* **1983**, *105*, 3341−3342.
(51) Matsumoto, K.; Miyamae, H.; Moriyama, H. *Inorg. Chem.* **1989**, *28*, 2959−2964.
(52) Matsumoto, K.; Sakai, K.; Nishio, K.; Tokisue, Y.; Ito, R.; Nishide, T.; Shichi, Y. *J. Am. Chem. Soc.* **1992**, *114*, 8110−8118.
(53) Villarroya, B. E.; Tejel, C.; Rohmer, M.-M.; Oro, L. A.; Ciriano, M. A.; Bénard, M. *Inorg. Chem.* **2005**, *44*, 6536−6544.